ADVANCED FUNCTIONAL MATERIALS
www.afm-journal.de

Fast Photoactuation Driven by Supramolecular Polymers Integrated into Covalent Networks

*S. Doruk Cezan, Chuang Li, Jacob Kupferberg, Luka Đorđević, Aaveg Aggarwal, Liam C. Palmer, Monica Olvera de la Cruz, and Samuel I. Stupp**

The design of robotic soft matter capable of emulating the complex movements of living organisms such as mechanical actuation, shape transformation, and autonomous translation remains a grand challenge in soft materials science. Functionalized hydrogels are excellent candidates for such materials since they can operate in water and are highly responsive to their environment, but their response times can be slow. This work investigates fast photoactuation of hybrid bonding hydrogels composed of peptide amphiphile (PA) supramolecular nanofibers bonded covalently to merocyanine-based (MCH^+) photoresponsive networks. By incorporating ionizable acrylic acid (AA) co-monomers in these networks, photoactuation at nearly neutral pH is observed, which in turn enables a new mechanism to accelerate the response by triggering the bundling of supramolecular nanofibers by rapid proton exchange reactions. Furthermore, this rapid response and its consequent large shape transformations lead to hydrogels capable of spontaneously tracking external light sources inspired by pedicellariae, defensive organs present in echinoderms like the starfish and the sea urchin. This work suggests that hybrid bonding polymers (HBPs), which leverage the interplay between supramolecular assemblies and covalent networks, offer novel strategies to design rapidly actuating soft robotic materials.

1. Introduction

Strategies to design robotic soft matter with the capacity to emulate sophisticated movements as well as dynamic shape and appearance transformations of living organisms are advancing rapidly.[1] Translational motion in particular among all the remarkable properties of living systems, has been of great interest in this regard as an essential component of life. From skeletal muscle fibers[2] to the intelligent tentacles of cephalopods,[3] the extraordinary behaviors and properties of active biological matter often emerge from the hierarchical self-assembly of nanoscopic building blocks. Given their similarity to living tissues, soft hydrogels have been a good target to emulate the sophisticated motility observed in biology.[1i,4] One reason responsive hydrogels are ideal candidates for designing life-like systems is their ability to exchange aqueous fluids in their environment as their molecular and supramolecular

S. D. Cezan, J. Kupferberg, A. Aggarwal, M. Olvera de la Cruz, S. I. Stupp
Department of Materials Science and Engineering
Northwestern University
2220 Campus Drive, Evanston, IL 60208, USA
E-mail: s-stupp@northwestern.edu

C. Li, L. Đorđević, L. C. Palmer, M. Olvera de la Cruz, S. I. Stupp
Simpson Querrey Institute
Northwestern University
303 East Superior Street, 11th floor, Chicago, IL 60611, USA

L. C. Palmer, M. Olvera de la Cruz, S. I. Stupp
Department of Chemistry
Northwestern University
2145 Sheridan Road, Evanston, IL 60208, USA

M. Olvera de la Cruz
Department of Chemical and Biological Engineering
Northwestern University
2145 Sheridan Road, Evanston, IL, USA

M. Olvera de la Cruz
Department of Physics and Astronomy
Northwestern University
2145 Sheridan Road, Evanston, IL, USA

S. I. Stupp
Department of Medicine
Northwestern University
676 North St. Clair Street, Chicago, IL 60611, USA

S. I. Stupp
Department of Biomedical Engineering
Northwestern University
2145 Sheridan Road, Evanston, IL 60208, USA

The ORCID identification number(s) for the author(s) of this article can be found under https://doi.org/10.1002/adfm.202400386

DOI: 10.1002/adfm.202400386

structure changes.[1j,4b,c,5] Many active materials can undergo chemical reactions, phase transitions, and shape transformations in response to a range of external stimuli like temperature,[4c,6] pH,[7] chemicals,[8] light,[1j,4d,6g,9] and magnetic fields,[1f,i,6g,10] have been reported in the literature. However, only a few previously investigated systems have successfully utilized mechanisms that take advantage of hierarchical structures to control shape changes and motion.[1j,4c,d] Among all hydrated polymer networks, "hybrid bonding polymers" (HBPs) in which both covalent and noncovalent bonding among structural units coexist is a wide-open field to combine the best of two worlds by integrating the dynamic behavior of supramolecular systems with the robustness of covalent polymer networks.[1j,4c,11] Our previous work on hierarchically structured hydrogels allowed for the design of thermo-responsive artificial muscles,[4c] and light-activated mechanical actuators.[1j] Supramolecular and hierarchical components contribute to stimulus-driven actuation in these systems by improving water diffusion[1j] and mechanical anisotropy.[4c] One aspect not considered so far in these systems is the role of dynamics in supramolecular assemblies across scales in enhancing the speed with which hybrid materials respond to an external stimulus.

In this work, we investigate how light-driven chemical reactions in the covalent network of an HBP affect the structure of supramolecular assemblies and its impact on actuation. We utilized for the study a spiropyran photoswitch which undergoes a chemical reaction from a charged hydrophilic form (protonated merocyanine, MCH^+) to an uncharged more hydrophobic cyclic form (spiropyran, SP) under illumination with white light (emitting between 380 and 700 nm and peaking at ≈480 nm).[1i] We investigated the effect of chemical composition in the covalent network and probed the effect of light exposure on mechanical actuation affected by the presence of supramolecular polymers in the HBP material. Experimentally we used video recordings of the hydrogels' actuation, scanning electron microscopy (SEM), confocal microscopy, rheology, and nanoindentation to understand the critical functional roles of supramolecular assemblies. This work highlights how soft robotic matter can draw from the synergistic interplay of covalent and supramolecular networks to develop rapidly actuating materials.

2. Preparation of Supramolecular-Covalent Hybrid Hydrogels

To prepare the covalent hydrogels, we mixed and photopolymerized *N*-isopropylacrylamide (NIPAM) monomer (**1**), *N*,*N*′-methylenebisacrylamide (MBA) crosslinking agent (**2**), acrylic acid (**3**), diphenyl(2,4,6-trimethylbenzoyl) phosphine oxide (TPO) photoinitiator (**4**), and merocyanine monomer (λ_{max} = 404 nm) (**5**) in a dioxane/water solution (**Figure 1a** and see Supporting Information Section 1). Scanning electron microscopy of this material revealed a high degree of porosity (≈28.9% with an average pore size of ≈9.4 μm^2), as shown in Figure 1b.

To prepare the supramolecular component of the HBP hydrogels, we first synthesized peptide amphiphile containing a polymerizable methacrylamide group (**PA1**) at the amino terminus (N terminus; $C_{16}V_3A_3E_3K$-methacrylamide) in order to make covalent connections between the supramolecular nanofibers and the covalent network. The PA nanofibers are formed by co-assembly of **PA 1** and non-functionalized **PA 2** ($C_{16}V_3A_3E_3$-NH_2) to control the density of methacrylamide groups on their surfaces (see Section S2, Supporting Information, for details). The 1:1 molar ratio of PA 1 to PA 2 was found to be optimal for achieving mechanical integration of the nanofibers with the photoactive polymeric network while still enabling the proton-driven muscle-like actuation provided by reversible bundling of nanofibers. Using nanofibers composed entirely of pure PA1, which would chemically and mechanically integrate the supramolecular nanofibers into the covalent network. However, this eliminates the degree of freedom necessary for fibers to bundle or contract in response to changes in surface charge. Conversely, nanofibers consisting solely of PA2 cannot be mechanically integrated with the covalent network, resulting in a slower and less effective contractual response (see Figure S14, Supporting Information). These nanofibers are then introduced into the covalent polymerization solution to create the HBP. SEM images of the HBP network revealed that pores (55.7% porosity with ≈3.1 μm^2 average pore size) formed by the covalent polymer appear to be filled with supramolecular nanofibers (Figure 1b). Confocal microscopy of the hybrid hydrogels shows that the covalent network (covalently labeled through copolymerization with molar ratio of 100:1 of NIPAAm to fluorescein O-methacrylate [green, λ_{abs} = 494 nm, λ_{em} = 512 nm in water]) is distributed nonuniformly resembling a porous structure throughout the material with regions in which PA nanofibers (covalently labeled through co-assembly with a molar ratio of 49.5:49.5:1 of PA 1, PA 2, and PA 3 [$C_{16}V_3A_3E_3K$-TAMRA, λ_{abs} = 555 nm, λ_{em} = 580 nm in water]) are clustered (see Section S3 and Figure S8, Supporting Information). However, the clusters appear yellow under merged channels, indicating the presence of interspersed covalent polymer within the nanofiber clusters. A higher-magnification SEM image reveals the presence of nanofiber bundles within the material, which are tens of micrometers in length and several micrometers in diameter (Figure 1b). Following synthesis of the hybrid hydrogels, they were punched into cross-shapes and were transferred into a glass tank filled with deionized (DI) water placed on an LED white light source (emitting between 380 and 700 nm peak at around 480 nm) to test their bending actuation performance (see Figure S2, Supporting Information, for ring-opening and ring-closing processes of the photoactive moiety). The performance of the gels was assessed by measuring the speed of actuation and the maximum bending angle reached. Interestingly, we found that the HBP hydrogels actuate faster and exhibit larger shape transformations than their covalent counterparts, indicating that the supramolecular component plays a role in actuation (Figure 1c).

3. Incorporation of Acrylic Acid Co-Monomers in Covalent Networks

The operating conditions for photoresponsive hydrogels based on spiropyran moieties are normally limited to low pH environments, thus limiting applications, particularly in contact with biological systems.[1j] This limitation is primarily due to the requirement of protonation of the spiropyran molecule (a weak

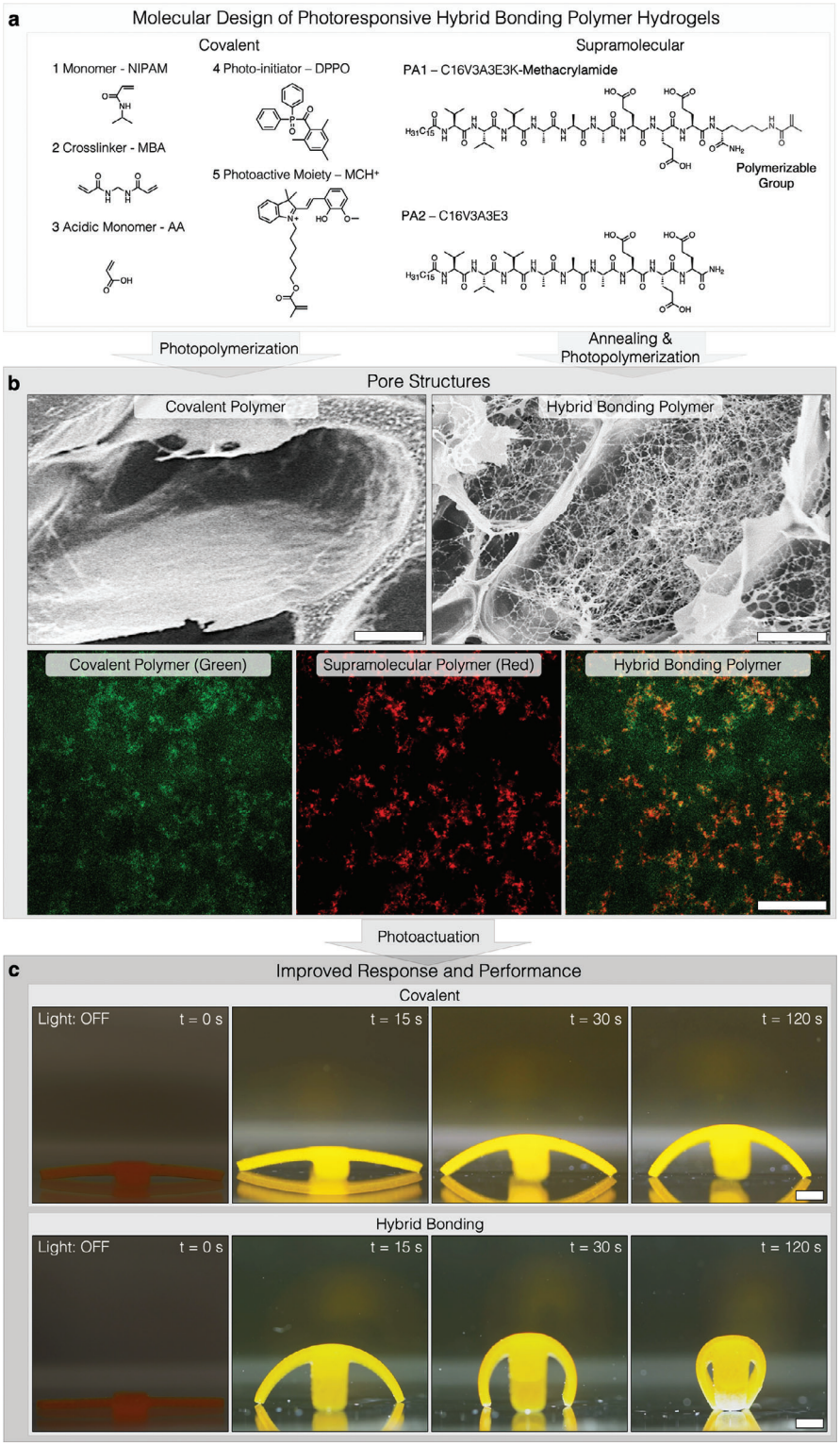

Figure 1. Synthesis of Covalent and Hybrid Bonding Polymer Actuators. a) Chemical structures of molecules used to synthesize the covalent network (left) and the supramolecular polymers (right). b) SEM images of the covalent network and the hybrid bonding polymer (Scale bar = 200 nm) (top), and confocal microscopy images (bottom) of a hybrid bonding hydrogel with crosslinked covalent network covalently labeled through copolymerization with fluorescein O-methacrylate (green) and PA nanofibers are covalently labeled through co-assembly with PA 3 ($C_{16}V_3A_3E_3K$-TAMRA) (red). PA nanofiber bundles appear yellow in color when merged channels are used (Scale bar is 20 μm; Objective lens is 60×). c) Photographs of cross-shaped objects prepared from the covalent network (top row) and the hybrid bonding polymer (bottom row) before visible light irradiation, and after 15, 30, and 120 seconds of exposure to light, reveal the difference in bending angle between the covalent and hybrid bonding polymers (Scale bar = 5 mm).

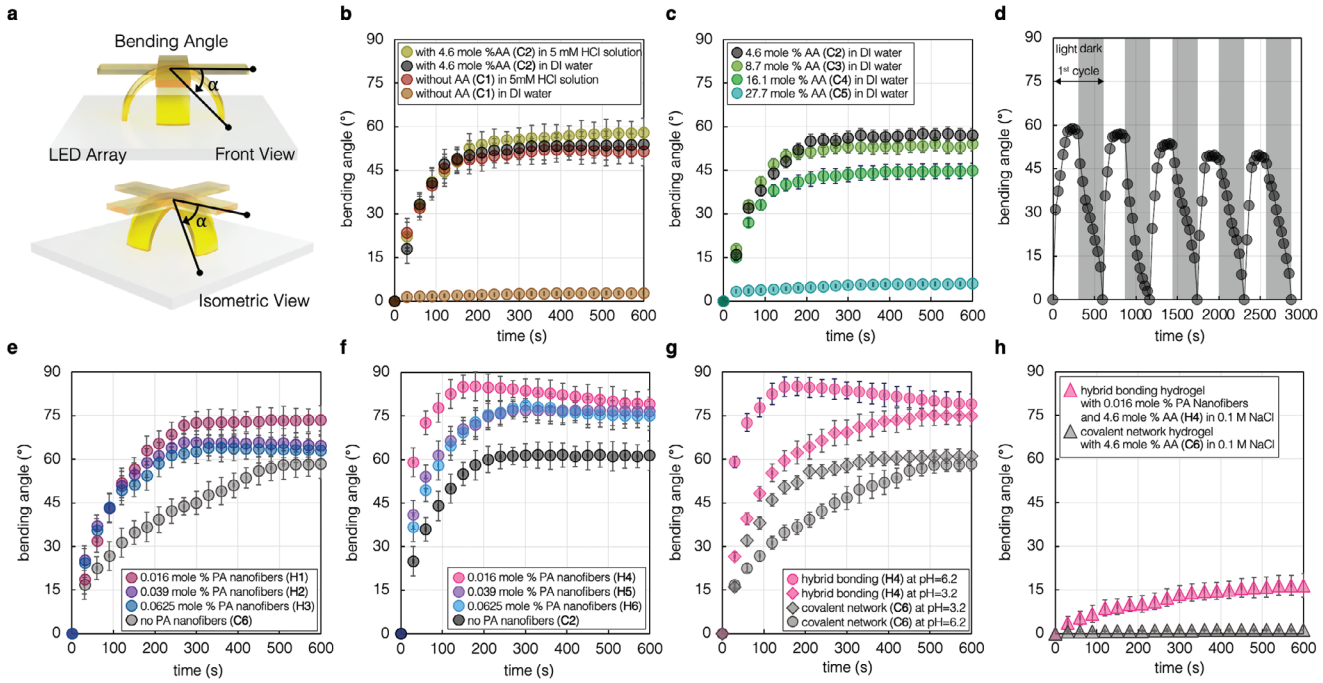

Figure 2. Photoactuation of hybrid hydrogel actuators. a) Schematic representation of the hydrogel actuator showing the definition of the photoinduced bending angle (α). b) Plot of bending angle during light exposure as a function of time in hydrogels containing 4.6 mol% acrylic acid (AA) co-monomer in 5 mM HCl solution, deionized water (DI), and under similar conditions for hydrogels that did not contain AA co-monomer. c) Plot of bending angle during light exposure as a function of time for hydrogels containing different amounts of AA co-monomer in DI water. d) Plot of bending angle change as a function of time over five light/dark cycles. e,f) Plots of bending angle during light irradiation as a function of time in hydrogels containing supramolecular PA nanofibers using 20:1 (e) and 30:1 (f) monomer to crosslinker molar ratios and 8.7 mol% AA co-monomer. g) Plot of bending angle during light irradiation as a function of time for hybrid hydrogels containing PA nanofibers and covalent network hydrogels immersed in solutions at various pH values. h) Plot of bending angle during light irradiation as a function of time for hybrid and covalent hydrogels immersed in 0.1 M NaCl solutions.

base), which stabilizes the photoresponsive merocyanine form (see Section S6 and Figure S17, Supporting Information). To circumvent this limitation we used the strategy previously reported by Ziółkowski et al.[12] and incorporated acrylic acid (AA) structural units into the covalent network. These structural units provide the necessary protons to switch the MCH^+ without altering the overall pH of the environment. We tested the actuation by recording the bending angle (α) change of cross-shaped 500–600 μm thick hydrogel films in a glass water tank illuminated from the bottom using a white LED array (**Figure 2a**). The composition of the polymers used in the study, along with their corresponding indices, is presented in **Table 1**. We studied the actuation response of covalent network hydrogels containing photoactive monomers substituted with a methoxy functional group incorporating acrylic acid (**C2**, 4.6 mol% AA) compared to control hydrogels without acrylic acid (**C1**). As expected on the basis of pH values (DI water pH ≈6.2; 5 mM HCl at pH ≈2.3), the hydrogels without AA in DI water did not actuate under illumination (Figure 2b). On the other hand, hydrogels incorporating AA structural units displayed substantial bending actuation. To validate our hypothesis on the role of acrylic acid for proton exchange from AA to MC, we performed similar experiments for both materials in an acidic (5 mM HCl at pH ≈2.3) solution. The control material without AA (**C1**) regained functionality displaying similar bending angles and response time as the material containing AA structural units (**C2**). This observation indicates that an acidic monomer in the covalent network provides enough protons to activate photoactive spiropyran moieties in DI water, thus not requiring the use of acidic media to drive actuation. We incorporated various concentrations of acidic monomers into the hydrogels in order to explore how the actuation depends on acrylic acid concentration in the covalent network and found maximal bending with 4.6 mol% (**C2**) to 8.7 mol% AA (**C3**) and lower bending angles at higher loading of 16.1 mol% (**C4**) to 27.1 mol% (**C5**) AA (Figure 2c). Our interpretation is that a high concentration of acidic monomers prevents the photoisomerization reaction by forcefully converting SP (weak base) to MCH^+ (photoacid). The actuation of AA-containing hydrogels is fully reversible over at least 20 cycles (see Supporting Information Figure S19, Supporting Information). The bending and flattening process of the covalent hydrogel (**C2**) with 4.6 mol% AA comonomer in DI water is given in Figure 2d. Initially, the actuators exhibited higher maximum bending angles (≈60° for covalent bonding hydrogel and ≈90° for hybrid bonding hydrogel), gradually decreasing until reaching a state of equilibrium between eighth and 20th cycles (≈50° (±4) for covalent bonding hydrogel and ≈81° (±3) for hybrid bonding hydrogel). We hypothesize that this phenomenon results from the initial release and migration of protons, followed by the establishment of equilibrium in local proton concentration and the distribution of charged polymer species within the hydrogel matrices. We next sought to understand this effect unique to HBPs in which supramolecular nanofibers formed by PA molecules were integrated with the photoactive covalent networks.

Table 1. List and composition of polymers used. All numbers represent mol%.

Index	Monomer	Crosslinker	Acidic Monomer	Photoinitiator	Photoactive Moiety	Supramolecular Nanofibers					
	NIPAM	MBA	AA	TPO	MCH+	PA1	PA1:PA2 3:1	PA1:PA2 1:1	PA1:PA2 1:3	PA2	PA4:PA5 1:1
C1	4.4	0.147	–	0.196	0.25	–	–	–	–	–	–
C2	4.4	0.147	4.6	0.196	0.25	–	–	–	–	–	–
C3	4.4	0.147	8.7	0.196	0.25	–	–	–	–	–	–
C4	4.4	0.147	16.1	0.196	0.25	–	–	–	–	–	–
C5	4.4	0.147	27.7	0.196	0.25	–	–	–	–	–	–
C6	4.4	0.22	4.6	0.196	0.25	–	–	–	–	–	–
C7	4.4	–	4.6	0.196	0.25	–	–	–	–	–	–
H1	4.4	0.22	4.6	0.196	0.25	–	–	0.016	–	–	–
H2	4.4	0.22	4.6	0.196	0.25	–	–	0.039	–	–	–
H3	4.4	0.22	4.6	0.196	0.25	–	–	0.0625	–	–	–
H4	4.4	0.147	4.6	0.196	0.25	–	–	0.016	–	–	–
H5	4.4	0.147	4.6	0.196	0.25	–	–	0.039	–	–	–
H6	4.4	0.147	4.6	0.196	0.25	–	–	0.0625	–	–	–
H7	4.4	0.147	4.6	0.196	0.25	–	–	–	–	–	0.016
H8	4.4	0.147	4.6	0.196	0.25	0.016	–	–	–	–	–
H9	4.4	0.147	4.6	0.196	0.25	–	0.016	–	–	–	–
H10	4.4	0.147	4.6	0.196	0.25	–	–	–	0.016	–	–
H11	4.4	0.147	4.6	0.196	0.25	–	–	–	–	0.016	–
H12	4.4	–	4.6	0.196	0.25	–	–	0.016	–	–	–

4. Incorporation of Supramolecular Nanofibers to Create Hybrid Bonding Hydrogels

We incorporated PA supramolecular nanofibers into the covalent polymer network to improve the hydrogel actuators' actuating response. This was motivated by earlier work in which we observed improved performance in a similar but different system.[1j] In the earlier work we observed greater bending angles under illumination relative to purely covalent networks. Based on computer simulations, we attributed this effect to the ability of the high aspect ratio nanofibers to drain out water molecules from the hydrogel as the covalent matrix becomes more hydrophobic under the influence of light. However, in the current work, we have observed a much faster-bending response when supramolecular hydrogel nanofibers were present with time scales on the order of one minute (as opposed to 10–20 min in earlier work[1j] as well as greater bending angles (Figure 2e,f and see Movie 2, Supporting Information). As described below, in order to establish the origin of these changes, we first had to investigate if hydrogels containing the supramolecular nanofibers had comparable mechanical properties to those composed only of covalent polymeric networks.

Adding PA nanofibers makes the hydrogels stiffer due to their persistence length and stiffness[1j] (see Section S5, Supporting Information), and in order to match the mechanical properties (viscoelastic behavior) similar to those of hydrogels containing only covalent polymeric networks we increased the monomer-to-crosslinker molar ratio from 20:1 to 30:1. We found 0.016 mol% PA nanofibers with the reduced crosslinker density (**H4**) have similar storage and loss moduli to the hydrogels with higher crosslinking density and without the PA nanofibers (**C6**) (see Figure S13, Supporting Information). When we compared the actuation of hydrogels with similar mechanical properties, we found that the actuation time to reach a ≈60° bending angle is 20-fold shorter (from 600 s to 30 s), and the maximum bending angle is increased from ≈58° (±5°) to ≈85° (±5°) (see Movie S1, Supporting Information). The decrease observed after reaching the maximum bending angle in the hybrid bonding hydrogels is attributed to the exposure of the non-irradiated (opposite) side. As the hydrogel approaches this maximum angle, the opposite side is exposed to light, resulting in actuation in the opposite direction and causing a slight opening. (see Supporting Information Section 3). To establish if the hybrid hydrogel (**H4**) can actuate in solutions with neutral pH and relatively high ion concentrations, we investigated the bending at different concentrations of salt and pH values. We found that raising the pH from 3.2 to 6.2 resulted in enhanced bending in the hybrid hydrogel, whereas we observed the opposite trend in hydrogels without the PA nanofibers (Figure 2g), suggesting that pH plays a role in the enhancement of bending. We hypothesize that this enhancement can be due to a second gradient. The effect of AA's presence in both covalent and HBP networks was investigated by comparing the actuation of structurally identical networks with a one-to-one molar ratio of AA and hydroxyethylmethacrylate (HEMA). HEMA was selected as a non-acidic and hydrophilic but non-ionic spaceholder monomer for AA in control materials. In one case, AA was integrated into the hydrogel networks and HEMA was introduced into the solution, while in another AA was added to the solution and HEMA was incorporated into the hydrogel networks. We found that the presence of HEMA, whether in solution or incorporated into the network, has no effect on actuation for both covalent and hybrid bonding networks. Our

findings show that in covalent networks, the initial presence of protons, whether from AA or elsewhere, does not significantly impact actuation. However, in hybrid bonding hydrogels, introducing protons through AA in solution decreases performance in great contrast to the fast actuation response when these units are incorporated into the covalent network. (see Figure S18, Supporting Information). This observation links the existence of a secondary actuation mechanism that generates a fast contraction to the related to the distribution of protons in the HBP. To establish the secondary stiffness gradient for fast actuation, nanofibers near the light source must become rapidly protonated when photoisomerization occurs. This is only possible if there is an excess of protons localized in that region of the film generated when merrocyanine units convert to spiropyran. In contrast, if PA nanofibers were to be protonated, and therefore bundled, due to the presence of soluble acid (HCl or AA monomer) homogeneously distributed throughout the hydrogel, the stiffness gradient which accelerates actuation would not be established. Based on our results and previous work,[12,13] it is also clear that the protons that are always available from ionization of AA structural units in the covalent network can catalyze photoconversion even at neutral pH. We suggest that protons in equilibrium with AA structural units of the covalent polymer are not as homogeneously distributed in the HBP as those of AA monomers or HCl. Thus, such protons do not to significantly protonate the supramolecular nanofibers and cause them to bundle in the absence of the light. This is the phenomenon that would precisely activate in the presence of the light the secondary contractile mechanism that leads to fast actuation. After the addition of 0.1 M NaCl, the hybrid hydrogels (**H4**) can still bend, despite reduced speed and bending angle, while actuation is completely eliminated in hydrogels without PA nanofibers (**C6**) (Figure 2h). This observation supports the hypothesis of a second gradient since a higher concentration of salt can screen charges and diminish the hydrophobicity gradient created by the photoconversion of MCH^+ (charged, hydrophilic) to SP (neutral, hydrophobic).

5. Light-Induced Stiffening of Hybrid Supramolecular-Covalent Hydrogels

To understand how supramolecular nanofibers improve the response and performance, we focused on possible chemical reactions between the supramolecular assemblies and the covalent network. We hypothesized that the actuation could be facilitated by proton exchange reactions between the photoactive moiety (MCH^+) and charged amino acid residues in the supramolecular assemblies. As photons enter the film surface near the light, the hydrophilic MCH^+ moieties partly convert to the hydrophobic SP form, thus releasing protons that can rapidly neutralize the glutamate residues in $C_{16}V_3A_3E_3$ monomers as well as acrylic acid structural units in the covalent network (**Figure 3a**, see Supporting Information for details of photochemical reaction mechanism). The photon-induced conversion of MCH^+ to SP in the network creates a gradient in which the hydrogel closest to the irradiated surface contains primarily hydrophobic SP moieties, while regions further away remain as charged MCH^+ groups. Similarly, a gradient of released protons could also develop in the hydrogel, locally neutralizing the negatively charged nanofibers, causing them to bundle and stiffen, which may contribute to actuation in addition to the hydrophobicity gradient. To validate this hypothesis, we prepared covalent polymer chains using the same formulation (**C2**) but without adding any crosslinking agent (**C7**) and found that the pH in these solutions decreased from ≈5.8 to ≈2.8 upon irradiation. The MCH^+ photoacids attached to polymer chains offer a means to measure the change in pH more accurately for two main reasons. First, protons generated by the photoacids within crosslinked hydrogel networks encounter hindered diffusion and dilution into the surrounding solution. Furthermore, the conditions within the hydrogel matrix can be replicated by dispersing the polymer chain in a solution whose volume is the same as the crosslinked hydrogel network counterpart, facilitating a more accurate pH measurement. Nevertheless, if we perform the same experiment using the HBP containing supramolecular nanofibers with no crosslinking agent (**H12**), a significant change in pH was not observed (Figure 3b). We suggest that this observation indicates that supramolecular nanofibers are being protonated and thus buffering pH. Proton transfer to the negatively charged supramolecular nanofibers would decrease electrostatic repulsion among them and lead to bundling and consequent changes to mechanical properties of the hydrogels. We have investigated previously the protonation of glutamic acid residues and resulting physical and morphological changes in PA nanofibers both experimentally and theoretically.[13] We also hypothesize that the reduction of repulsive forces facilitates buckling and entanglement among nanofibers and so overall one expects a contraction of the hydrogel (Figure 3f and Movie S3, Supporting Information). Nanofiber bundles exhibit higher light scattering (opacity) than dispersed counterparts, which provides strong evidence for the bundling of PA nanofibers within the hybrid bonding hydrogels. To test this hypothesis, we conducted transmission UV-vis experiments at 600 nm (Tyndall Effect) to assess light scattering before and after irradiation. Our findings revealed that HBP hydrogels scatter ≈3.71 times more light after irradiation, whereas covalent hydrogels exhibit a much smaller change (≈1.08 times) in light scattering (Figures S15 and S16, Supporting Information). The photoinduced proton exchange from the covalent network to the supramolecular nanofibers could therefore contribute synergistically to actuation along with dehydration caused by the chemical conversion from the hydrophilic merocyanine moieties to the hydrophobic spiropyran structure. We propose therefore that this synergy could explain the observed improvement in actuation performance relative to our earlier results on different but very similar hydrogels undergoing actuation at low rather than neutral pH.[1j] In our earlier hybrid bonding systems containing PA nanofibers,[1j] the permanent acidic pH of ≈2.3 during actuation experiments would keep nanofibers in a highly bundled or entangled structure. In fact, in our previous work, confocal microscopy revealed the presence of bundled fibers throughout the hybrid bonding material, seemingly forming a hierarchical structure at larger length scales.[1j] In this context we would expect that additional protons generated by the photochemistry would not lead to major contractile changes in the material's microstructure that contribute further to actuation. However, in the system investigated here we were able to keep the hydrogel in a neutral pH environment without interfering with the photoconversion reaction given the availability of catalytic

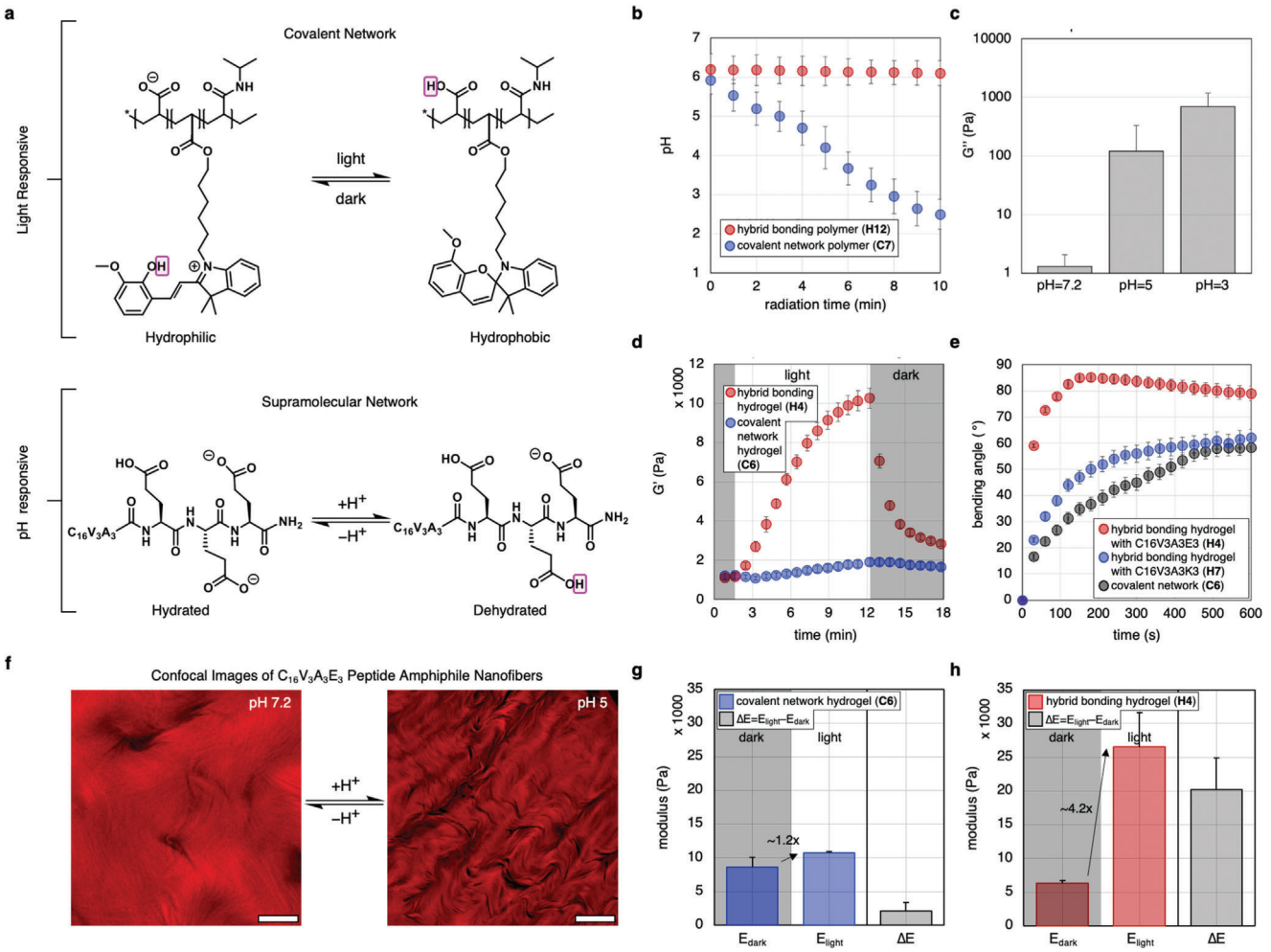

Figure 3. a) Proton exchange to an acrylic acid structural unit in the covalent network upon photoisomerization of the merocyanine dye moiety to spiropyran (top), or to ionized glutamic acid residues in peptide amphiphile monomers of supramolecular nanofibers (bottom). b) Plot of the pH of solutions surrounding a covalent polymer (with 4.6 mol% acrylic acid) or the hybrid hydrogel containing supramolecular nanofibers (with 0.016 mol% $C_{16}V_3A_3E_3$ nanofibers and 4.6 mol% acrylic acid) measured during light illumination for 10 minutes. c) Bar graph of loss moduli of physical gels composed of supramolecular nanofibers (4 wt%) alone at various pH values. d) Plot of storage modulus in a covalent and a hybrid hydrogel during illumination with visible light for 10 min and under dark conditions. e) Plot of bending angle under light irradiation as a function of time in two hybrid hydrogels one containing an anionic monomer in the supramolecular nanofiber ($C_{16}V_3A_3E_3$) and second one containing a cationic monomer in its nanofibers ($C_{16}V_3A_3K_3$). f) Confocal images displaying the morphology of supramolecular 5-TAMRA-labeled PA $C_{16}V_3A_3E_3$ nanofibers (co-assembled with a molar ratio of 49.5:49.5:1 of PA 1, PA 2, and PA 3) in high pH (≈7.2) and low pH (≈5). At pH 7.2, PA nanofiber bundles exhibit an extended structure, while at pH 5, PA nanofibers are observed to be more contracted and bundled. Scale bars are 100 μm. Objective lens is 60×. g) Elastic modulus of covalent network hydrogels measured using nanoindentation before and after illumination with visible light for 15 s. h) Elastic modulus of hybrid bonding hydrogels measured using nanoindentation before and after illumination with visible light (48 mW cm^{-2}) for 15 s.

protons from acrylic acid monomer. Thus, in addition to the gradient in photoconversion near the light source, the lower degree of E residue protonation in the supramolecular nanofibers at neutral pH can also generate a second gradient in the density of hierarchical structures. Our hypothesis is therefore that both of these gradients accelerate jointly the contraction that bends the hydrogel.

To investigate how the mechanical properties of PA hydrogels change with pH, we carried out rheological measurements. We found that the loss modulus of a nanofiber gel (1 wt%) increased from pH ≈7.2 to pH ≈5 and reached a maximum value at pH 3 (Figure 3c). At pH values below 3 (at pH ≈1), PA nanofibers precipitate from solution, forming macroscopic bundles and evidenced by the presence of opaque regions and inconsistent solution flow (Supporting Information Figure S15). Confocal microscopy images show the effect of pH on the morphology of the $C_{16}V_3A_3E_3$ PA nanofibers (covalently labeled covalently labeled through co-assembly with PA 3 ($C_{16}V_3A_3E_3K$-TAMRA), red) (Figure 3f). We also measured the storage modulus change under illumination to establish if light-induced stiffening occurs in the hybrid materials. We found that the stiffness of the HBP increases significantly from ≈1.5 kPa to ≈10.2 kPa and becomes much higher than the stiffness of the covalent network. The storage modulus decreases under dark conditions which

we interpret as a result of the deprotonation of glutamic acid residues on PA nanofibers as of spiropyran residues convert back to merocyanine in the covalent network. The covalent network, on the other hand, just undergoes a rather small change from ~1.5 kPa to ~1.9 kPa during light exposure (Figure 3d). The storage modulus of the covalent network increases under light exposure due to dehydration and decreases in the dark due to rehydration. To measure the difference in elastic modulus between the light-irradiated surface and the surface that remained unexposed to light, we conducted nanoindentation experiments. We observed a significant increase in the stiffness of the HBP surface, rising from ≈6.4 kPa to ≈26.6 kPa within 15 seconds of light irradiation (Figure 3g), which is a significantly greater difference compared to the covalent network, where the surface stiffness increased from ≈8.7 kPa to ≈10.8 kPa under the same conditions (Figure 3h). To further verify the proton exchange between the covalent and supramolecular networks, we incorporated supramolecular nanofibers composed of PA molecules in which the peptide segment terminates with three lysine residues which can be protonated to become positively charged (formed by co-assembly of 1:1 ratio of **PA 4** ($C_{16}V_3A_3K_3$- K(methacrylic acid)) and non-functionalized **PA 5** ($C_{16}V_3A_3K_3$)), instead of three glutamic acid residues ($C_{16}V_3A_3E_3$). In HBP-containing nanofibers with K3 terminated PA molecules (**H7**) proton exchange between the covalent network and the supramolecular assemblies would lead to an increase in their charge density which in turn would decrease or suppress bundle formation. Therefore, the proposed light-induced stiffening mechanism as a result of a decreasing pH in the $C_{16}V_3A_3E_3$-containing hybrid (**H4**) would not occur. Indeed, we found that the hybrid bonding hydrogels containing PA molecules with glutamic acid residues have a faster actuation response and higher maximum bending angles compared to those with lysine-charged groups ($C_{16}V_3A_3K_3$) (Figure 3e). The slight improvement of response in HBP with positively charged supramolecular nanofibers (**H7**) is presumably the result of water transport by supramolecular nanofibers, as proposed in our previous works.[1j] It is also important to note that if we compare the response of HBP actuators described in this work with the one described previously[1j] (using the same SP molecule), the one in this work is 120-fold faster with a significantly high maximum bending angle compared to the previous one (Movie S2, Supporting Information). Based on this evidence, we propose that MCH^+ is acting as a photoacid that protonates the glutamic acid groups on the nanofibers and the acrylic acid monomers, enhancing the stiffness gradient generated by the covalent network as a result of light-driven water loss resulting from chemical conversion (Figure 3a; Supporting Information Section 6).

6. A Bio-Inspired Light Tracking Claw

To demonstrate how the hydrogels investigated here can be used for soft robotics, we created an autonomous light-tracking claw inspired by the tiny pincers of echinoderms known as pedicellaria[14] (**Figure 4a**, see Section S7, Supporting Information, for details). Our hydrogel claw can regulate its motion by bending phototactically and closing the claw that receives the highest light intensity. The observed self-regulation of the claw is enabled by a negative feedback loop created by self-shadowing of the stalk when the claw reaches the optimum bending angle. The feedback through dehydration/rehydration cycles provides stabilization at a given metastable position in light-tracking motion and, therefore, the continuous autonomous operation of the claw. Illuminating one side of the gel actuators leads to its contraction and the bending of the stalk toward the light source, which continues until the claws (which also bend as a result of the photoactuation) cast a shadow (light intensity at ≈4.7 mW cm^{-2}) on the hydrogel (see Figure 4b). The shadow leads to a lower rate of contraction relative to the expansion rate, therefore, the gel stalk rehydrates, swells, and bends away from the light source. However, as the claw moves, the stalk is illuminated again. The periods of illumination and shadow lead to cycles of bending and straightening mediated by the feedback within the material. This dynamic process enables the claw to track the light source continuously and precisely in any direction (Figure 4b; see Movie S4, Supporting Information). We measured the light tracking performance of the hydrogel composed entirely of a covalent network versus that of a hydrogel containing the supramolecular nanofibers by placing the light source at a 90° angle to the claw's normal. We found that the hybrid bonding hydrogel (covalent network plus supramolecular nanofibers) tracks light significantly faster (approximately six times faster to reach the maximum bending angle) compared to the covalent network. In contrast to the hybrid bonding hydrogel claw, the covalent network hydrogel has a lower capacity to bend, limiting its ability to track light sources (Figure 4c). We also checked the responsiveness of the light-tracking claw to incident light at various angles. In these experiments, we found that the hybrid bonding material closely tracks the incident light, whereas the covalent network gel cannot achieve high deflection angles (Figure 4d). These results indicate that the incorporation of the supramolecular nanofibers enables a light-tracking claw with faster actuation, accuracy, and performance. In contrast, the covalent network gel cannot keep up at higher elevation angles, indicating that incorporating supramolecular nanofibers yields an autonomous light-tracking claw with faster actuation, accuracy, and performance (Figure 4d).

7. Conclusion

This study demonstrates the interplay that can occur between covalent networks and supramolecular assemblies in HBPs to generate robotic materials with fast actuation capacity. We achieved enhancement of actuation by incorporating peptide amphiphile supramolecular nanofibers that make covalent bonds with spiropyran-based covalent networks containing acidic co-monomers. The acidic co-monomers enable light-driven actuation at neutral pH, which leads to proton transfer from the covalent network to anionic supramolecular nanofibers. This transfer leads to contraction and stiffening of the supramolecular component causing greater and faster bending actuation. As a functional proof of principle, we used the hybrid bonding hydrogels to design a bioinspired robotic material with light-tracking claws. Overall, this work highlights the potential design space for biomimetic autonomous robotic functions offered by soft materials that incorporate both polymeric networks and supramolecular assemblies.

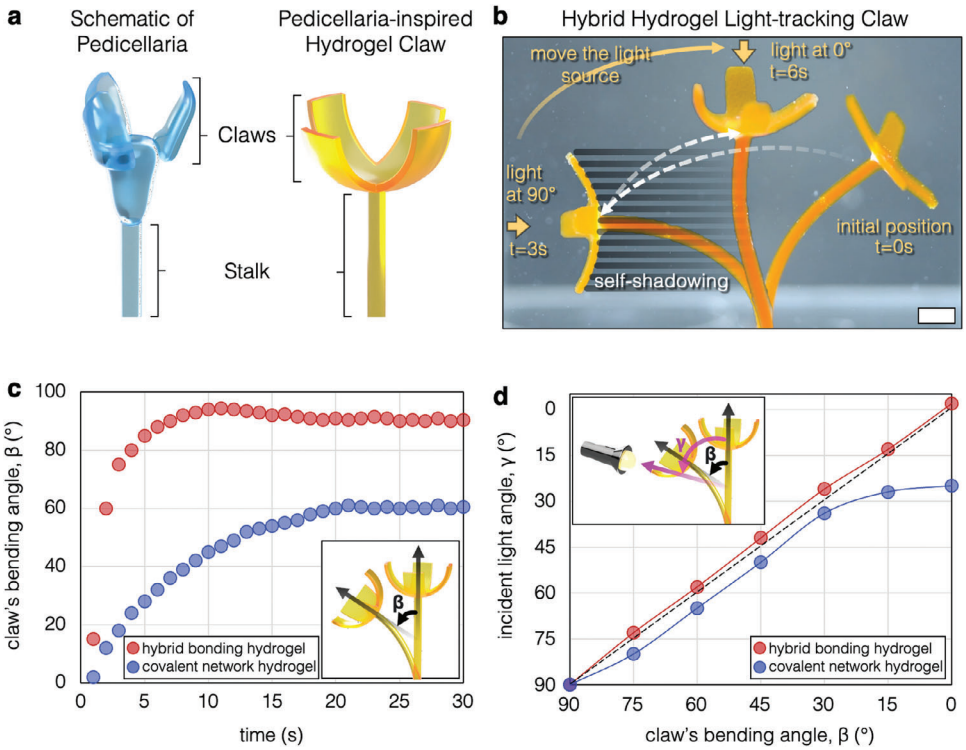

Figure 4. Pedicellaria-inspired light-tracking hybrid hydrogel claw. a) Schematic illustrations of the anatomy of trifoliate pedicellaria and of a corresponding pedicellaria-inspired hydrogel claw. b) Overlayed photographic snapshots of the pedicellaria-inspired light-tracking claw following the light source; the dark lines on the snapshots indicate the self-shadowing of the claws at 90° and the claw follows the light source as it moves from 90° to 0° (scale bar = 5 mm). c) Plot of the claw's principal axis angle ß change from its original position (see inset) under irradiation from left side ($\beta = 90°$) for a hybrid (red) and a covalent network hydrogel (blue). d) Plot of the incident light angle (γ) as a function of the angle of the claw's normal (δ) for a claw made out of a covalent network (blue) and another made of a hybrid hydrogel containing supramolecular nanofibers (red) (shown schematically in the inset); the ideal light tracker line is for $\delta = \gamma$ (yellow).

Supporting Information

Supporting Information is available from the Wiley Online Library or from the author.

Acknowledgements

This work made use of the IMSERC at Northwestern University, which has received support from the NIH (1S10OD012016-01/1S10RR019071-01A1), Soft and Hybrid Nanotechnology Experimental (SHyNE) Resource (NSF ECCS-1542205), the State of Illinois, and the International Institute for Nanotechnology (IIN). This work also made use of the MatCI Facility, which receives support from the MRSEC Program (NSF DMR-1720139) of the Materials Research Center at Northwestern University. This work was supported by the Center for Bio-Inspired Energy Science (CBES), an Energy Frontier Research Centers funded by the U.S. Department of Energy (DOE), Office of Science, Basic Energy Sciences under award number DE-SC0000989. S.D.C. acknowledges support from Northwestern University through a Ryan Fellowship.

Conflict of Interest

The authors declare no conflict of interest.

Author Contributions

S.D.C. developed and prepared materials, designed and performed all the experiments, conducted data analysis, and wrote the manuscript. C.L. synthesized spiropyran molecules, provided assistance, and took part in discussions in the initial stages of the work. J.K. contributed to rheology experiments and sample preparation for scanning electron microscopy experiments. L.D. synthesized spiropyran molecules and took part in discussions to understand the mechanism. L.C.P. took part in discussions and wrote the manuscript. A.A. and M.O.d.l.C. provided insight in discussions. S.I.S. directed the research and wrote the manuscript.

Data Availability Statement

The data that support the findings of this study are available from the corresponding author upon reasonable request.

Keywords

autonomous motion, dynamic behavior, hybrid bonding polymers, hydrogel actuators, photoresponsive, soft robotics, supramolecular nanofibers

Received: May 24, 2024
Published online:

[1] a) R. Pfeifer, M. Lungarella, F. Iida, *Science* **2007**, *318*, 1088; b) A. J. Ijspeert, *Science* **2014**, *346*, 196; c) J. Aizenberg, P. Fratzl, *Adv. Funct.*

Mater. **2013**, *23*, 4398; d) G. M. Whitesides, *Interface Focus* **2015**, *5*, 20150031; e) U. G. K. Wegst, H. Bai, E. Saiz, A. P. Tomsia, R. O. Ritchie, *Nat. Mater.* **2015**, *14*, 23; f) W. Q. Hu, G. Z. Lum, M. Mastrangeli, M. Sitti, *Nature* **2018**, *554*, 81; g) O. Dumele, J. H. Chen, J. V. Passarelli, S. I. Stupp, *Adv. Mater.* **2020**, 32; h) S. J. Park, M. Gazzola, K. S. Park, S. Park, V. Di Santo, E. L. Blevins, J. U. Lind, P. H. Campbell, S. Dauth, A. K. Capulli, F. S. Pasqualini, S. Ahn, A. Cho, H. Y. Yuan, B. M. Maoz, R. Vijaykumar, J. W. Choi, K. Deisseroth, G. V. Lauder, L. Mahadevan, K. K. Parker, *Science* **2016**, *353*, 158; i) C. Li, G. C. Lau, H. Yuan, A. Aggarwal, V. L. Dominguez, S. Liu, H. Sai, L. C. Palmer, N. A. Sather, T. J. Pearson, D. E. Freedman, P. K. Amiri, M. Olvera de la Cruz, S. I. Stupp, *Sci Robot* **2020**, 5; j) C. Li, A. Iscen, H. Sai, K. Sato, N. A. Sather, S. M. Chin, Z. Alvarez, L. C. Palmer, G. C. Schatz, S. I. Stupp, *Nat. Mater.* **2020**, *19*, 900.

[2] a) W. R. Frontera, J. Ochala, *Calcif. Tissue Int.* **2015**, *96*, 183; b) K. Mukund, S. Subramaniam, *Wiley Interdiscip. Rev. Syst. Biol. Med* **2020**, 12.

[3] a) S. L. Hooper, *Curr. Biol.* **2020**, *30*, R1301; b) K. Knight, *J. Exp. Biol.* **2021**, 224.

[4] a) C. Li, Y. G. Xue, M. D. Han, L. C. Palmer, J. A. Rogers, Y. G. Huang, S. I. Stupp, *Matter* **2021**, *4*, 1377; b) C. Li, A. Iscen, L. C. Palmer, G. C. Schatz, S. I. Stupp, *J. Am. Chem. Soc.* **2020**, *142*, 8447; c) S. M. Chin, C. V. Synatschke, S. Liu, R. J. Nap, N. A. Sather, Q. Wang, Z. Alvarez, A. N. Edelbrock, T. Fyrner, L. C. Palmer, I. Szleifer, M. Olvera de la Cruz, S. I. Stupp, *Nat. Commun.* **2018**, *9*, 2395; d) J. W. Chen, F. K. C. Leung, M. C. A. Stuart, T. Kajitani, T. Fukushima, E. van der Giessen, B. Feringa, *Nat. Chem.* **2018**, *10*, 132; e) H. Na, Y. W. Kang, C. S. Park, S. Jung, H. Y. Kim, J. Y. Sun, *Science* **2022**, *376*, 301; f) S. Craig, *Science* **2019**, *363*, 451.

[5] Y. S. Zhang, A. Khademhosseini, *Science* **2017**, 356.

[6] a) C. H. Chen, L. C. Palmer, S. I. Stupp, *Nano Lett.* **2018**, *18*, 6832; b) A. Dallinger, P. Kindlhofer, F. Greco, A. M. Coclite, *ACS Appl. Polym. Mater.* **2021**, *3*, 1809; c) C. Wang, N. T. Flynn, R. Langer, *Adv. Mater.* **2004**, *16*, 1074; d) R. Zhang, H. K. Mjoseng, M. A. Hoeve, N. G. Bauer, S. Pells, R. Besseling, S. Velugotla, G. Tourniaire, R. E. B. Kishen, Y. Tsenkina, C. Armit, C. R. E. Duffy, M. Helfen, F. Edenhofer, P. A. de Sousa, M. Bradley, *Nat. Commun.* **2013**, 4; e) B. Hashmi, L. D. Zarzar, T. Mammoto, A. Mammoto, A. Jiang, J. Aizenberg, D. E. Ingber, *Adv. Mater.* **2014**, *26*, 3253; f) Z. X. Zhang, K. L. Liu, J. Li, *Angew. Chem Int. Ed. Engl.* **2013**, *52*, 6180; g) F. G. Downs, D. J. Lunn, M. J. Booth, J. B. Sauer, W. J. Ramsay, R. G. Klemperer, C. J. Hawker, H. Bayley, *Nat. Chem.* **2020**, *12*, 363.

[7] a) P. Gupta, K. Vermani, S. Garg, *Drug Discovery Today* **2002**, *7*, 569; b) D. Schmaljohann, *Adv. Drug Delivery Rev.* **2006**, *58*, 1655; c) L. D. Zarzar, J. Aizenberg, *Acc. Chem. Res.* **2014**, *47*, 530; d) L. D. Zarzar, P. Kim, J. Aizenberg, *Adv. Mater.* **2011**, *23*, 1442.

[8] a) A. Grinthal, J. Aizenberg, *Chem. Soc. Rev.* **2013**, *42*, 7072; b) X. M. He, M. Aizenberg, O. Kuksenok, L. D. Zarzar, A. Shastri, A. C. Balazs, J. Aizenberg, *Nature* **2012**, *487*, 214.

[9] a) S. Sur, J. B. Matson, M. J. Webber, C. J. Newcomb, S. I. Stupp, *ACS Nano* **2012**, *6*, 10776; b) Y. S. Zhao, C. Xuan, X. S. Qian, Y. Alsaid, M. T. Hua, L. H. Jin, X. M. He, *Sci. Rob.* **2019**, 4; c) D. R. Morim, A. Meeks, A. Shastri, A. Tran, A. V. Shneidman, V. V. Yashin, F. Mahmood, A. C. Balazs, J. Aizenberg, K. Saravanamuttu, *Proc. Natl. Acad. Sci. USA* **2020**, *117*, 3953; d) K. Sumaru, K. Ohi, T. Takagi, T. Kanamori, T. Shinbo, *Langmuir* **2006**, *22*, 4353; e) R. Klajn, *Chem. Soc. Rev.* **2014**, *43*, 148; f) L. Kortekaas, W. R. Browne, *Chem. Soc. Rev.* **2019**, *48*, 3406; g) L. Li, J. M. Scheiger, P. A. Levkin, *Adv. Mater.* **2019**, *31*, 1807333; h) C. Berton, C. Pezzato, *Eur. J. Org. Chem.* **2023**, *26*, 202300070.

[10] Z. Y. Ren, W. Q. Hu, X. G. Dong, M. Sitti, *Nat. Commun.* **2019**, 10.

[11] a) Z. Yu, F. Tantakitti, T. Yu, L. C. Palmer, G. C. Schatz, S. I. Stupp, *Science* **2016**, *351*, 497; b) T. D. Clemons, S. I. Stupp, *Prog. Polym. Sci.* **2020**, *111*, 101310; c) E. P. Bruckner, T. Curk, L. Dordevic, Z. W. Wang, Y. Yang, R. M. Qiu, A. J. Dannehoffer, H. Sai, J. Kupferberg, L. C. Palmer, E. Lujiten, S. I. Stupp, *ACS Nano* **2022**, *16*, 8993.

[12] B. Ziolkowski, L. Florea, J. Theobald, F. Benito-Lopez, D. Diamond, *Soft Matter* **2013**, *9*, 8754.

[13] a) J. E. Goldberger, E. J. Berns, R. Bitton, C. J. Newcomb, S. I. Stupp, *Angew. Chem Int. Ed. Engl.* **2011**, *50*, 6292; b) R. J. Nap, B. F. Qiao, L. C. Palmer, S. I. Stupp, M. Olvera de la Cruz, I. Szleifer, *Front Chem* **2022**, 10; c) T. J. Moyer, J. A. Finbloom, F. Chen, D. J. Toft, V. L. Cryns, S. I. Stupp, *J. Am. Chem. Soc.* **2014**, *136*, 14746; d) M. P. Hendricks, K. Sato, L. C. Palmer, S. I. Stupp, *Acc. Chem. Res.* **2017**, *50*, 2440; e) N. A. Sather, H. Sai, I. R. Sasselli, K. Sato, W. Ji, C. V. Synatschke, R. T. Zambrotta, J. F. Edelbrock, R. R. Kohlmeyer, J. O. Hardin, J. D. Berrigan, M. F. Durstock, P. Mirau, S. I. Stupp, *Small* **2021**, *17*, 2005743.

[14] R. L. Turner, J. M. Boucher, B. O. O'Neill, N. W. Becker, *Zoomorphology* **2021**, *140*, 505.